

Modern Physics Letters A
 © World Scientific Publishing Company

Single/Double-Spin Asymmetry Measurements of Semi-Inclusive Pion Electroproduction on a Transversely Polarized ^3He Target through Deep Inelastic Scattering

Xin Qian*

on behalf of the Jefferson Lab
 Hall A Collaboration and E06-010 Collaboration

*Kellogg Radiation Laboratory, California Institute of Technology,
 1200 East California Boulevard, Pasadena, California 91125, U.S.A.*

Received (Day Month Year)

Revised (Day Month Year)

Parton distribution functions, which represent the flavor and spin structure of the nucleon, provide invaluable information in illuminating quantum chromodynamics in the confinement region. Among various processes that measure such parton distribution functions, semi-inclusive deep inelastic scattering is regarded as one of the golden channels to access transverse momentum dependent parton distribution functions, which provide a 3-D view of the nucleon structure in momentum space. The Jefferson Lab experiment E06-010 focuses on measuring the target single and double spin asymmetries in the $^3\text{He}(e, e'\pi^{\pm})X$ reaction with a transversely polarized ^3He target in Hall A with a 5.89 GeV electron beam. A leading pion and the scattered electron are detected in coincidence by the left High-Resolution Spectrometer at 16° and the BigBite spectrometer at 30° beam right, respectively. The kinematic coverage concentrates in the valence quark region, $x \sim 0.1-0.4$, at $Q^2 \sim 1-3 \text{ GeV}^2$. The Collins and Sivers asymmetries of ^3He and neutron are extracted. In this review, an overview of the experiment and the final results are presented. Furthermore, an upcoming 12-GeV program with a large acceptance solenoidal device and the future possibilities at an electron-ion collider are discussed.

Keywords: SIDIS; SSA; TMDs; Nucleon Spin Structure; PDF.

PACS Nos.: include PACS Nos.

1. Introduction

One of the important tasks of nuclear physics has been and still is to understand the internal structure of nucleons in terms of quarks and gluons, which are the fundamental degrees of freedom of Quantum Chromodynamics (QCD). QCD, the widely accepted theory of the strong interaction, has been well-tested through perturbative calculations at high energies where quarks and gluons behave like free particles^{1,2}. However, perturbative calculations break down at low energies, where colored quarks

*email:xqian@caltech.edu

and gluons are bounded inside colorless hadron, since the strong interaction coupling constant increases with the decrement of the energy scale. Therefore, the internal structure of nucleons still remains illusive. Although a full description of nucleon structure is not calculable yet, experimental measurements of the universal parton distribution functions (PDFs)³ have provided unique and quantitative information about the partonic dynamics. PDFs, which are probability densities of finding a parton inside a hadron, bridge nucleons and their partonic structure together with the fragmentation functions (FFs), which are probability densities that a parton hadronize into a hadron. In particular, the energy evolution of PDFs has been one of the best tests of QCD.

In the leading twist, there are three quark distribution functions after integrating over the quark transverse momentum: the unpolarized PDF f_1 , the longitudinal polarized PDF g_1 , and the quark transversity PDF h_1 . Through several decades of experimental and theoretical efforts³, the unpolarized PDF f_1 has been extracted with an excellent precision over a large range of x and Q^2 from DIS, Drell-Yan, and other processes. With advances in experimental techniques of polarizing leptons and nucleons⁴, the longitudinal polarized PDF g_1 has also been extracted with a reasonable precision over a range of x and Q^2 . The least known among these three PDFs is the chirally odd transversity PDF h_1 , which was initially discussed by Hidaka, Monsay, and Sivers⁵ in 1978, by Ralston and Soper⁶ in 1979, and later by Jaffe and Ji⁷ in early 1990s. The lowest moment of h_1 is called the “tensor charge”, which is a fundamental property of the nucleon, and has been calculated from lattice QCD⁸ and various models^{9,10,11,12,13,14}. Transversity is further constrained by Soffer’s inequality¹⁵, $|h_1^q| \leq \frac{1}{2}(f_1^q + g_1^q)$, which holds under the next-to-leading-order QCD evolution^{16,17,18}. However, a possible violation of Soffer’s bound has been suggested¹⁹.

Compared to the collinear PDF f_1 , g_1 , and h_1 , their corresponding TMDs depend not only on the longitudinal momentum fraction x , but also on the parton transverse momentum k_T . TMDs provide a full 3-D view of the nucleon structure in momentum space. For example, an intuitive interpretation of the unpolarized TMD f_1 is that it represents the probability of finding a parton inside a nucleon with a longitudinal momentum fraction x and a transverse momentum k_T . Beside TMDs f_1 , g_1 , and h_1 , there are five more transverse momentum dependent distribution functions (TMDs) in the leading twist^{20,21,22}. They are the Sivers function f_{1T}^\perp , the Boer Mulders function h_1^\perp , the transversal helicity function g_{1T}^\perp , the longitudinal transversity function h_{1L}^\perp , and the pretzelosity functions h_{1T}^\perp . All eight TMDs and their isospin structure have been studied in the large- N_c QCD²³. Furthermore, these additional five TMDs require interferences between wave function components with different amounts of orbital angular momentum (OAM)^{24,25}, and thus require non-zero OAM. The Sivers function f_{1T}^\perp (the Boer Mulders function h_1^\perp) provides information about the correlation between the quark OAM and the nucleon (the quark) spin. In comparison, the longitudinal function g_{1L} and the

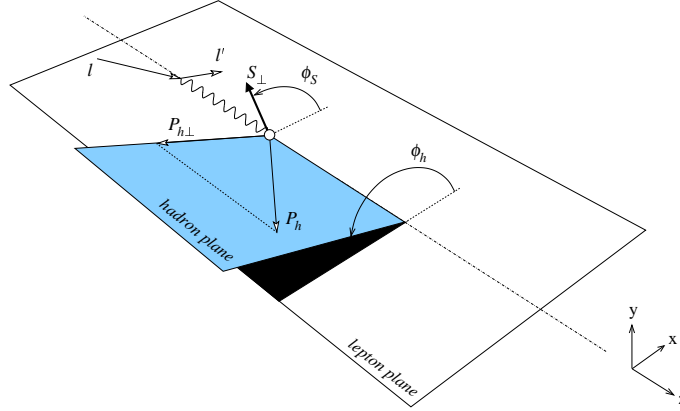


Fig. 1. Definitions of the azimuthal angle ϕ_h and ϕ_S , and the hadron transverse momentum for SIDIS process in the nucleon-at-rest frame following the Trento convention²⁶. Here, l , l' , P_h , and S_{\perp} represent the momenta of the initial lepton, the scattered lepton, the leading hadron, and the spin vector of the initial nucleon, respectively.

transversity function h_{1T} describe correlations between the quark spin and the nucleon spin. Furthermore, the Sivers function f_{1T}^{\perp} and the Boer Mulders function h_{1T}^{\perp} are T-odd functions, which rely on the final state interactions (FSI) experienced by the active quark in semi-inclusive DIS (SIDIS) process as both functions vanish without FSI. On the other hand, the transversal helicity function g_{1T} , the longitudinal transversity function h_{1L}^{\perp} and the pretzelosity functions h_{1T}^{\perp} are T-even and as a result do not require FSI to be nonzero. The wealth of information from all these functions could thus provide invaluable information about the quark orbital angular momentum.

2. Single and Double Spin Asymmetries in SIDIS

Compared to inclusive DIS process, in which only the scattered lepton is detected, SIDIS process $N(l, l'h)X$ also requires detection of one of the leading hadrons fragmented from the struck quark. By using the leading hadron to tag the flavor, the spin, and the transverse momentum information of the struck quark, SIDIS process provides unique sensitivities to TMDs. Fig. 1 shows the kinematics of SIDIS process following the Trento convention²⁶. The SIDIS reaction is regarded as one of the golden channels to access TMDs, since it can access all eight leading twist TMDs with different combinations of beam and target polarizations²².

For example, the angular dependence of the single spin asymmetry (SSA) A^{SSA} in the scattering of an unpolarized lepton beam off a transversely polarized target is:

$$\begin{aligned}
 A^{SSA}(\phi_h, \phi_S) &= \frac{1}{P_T} \frac{Y_{\phi_h, \phi_S} - Y_{\phi_h, \phi_S + \pi}}{Y_{\phi_h, \phi_S} + Y_{\phi_h, \phi_S + \pi}} \\
 &\approx A_C \sin(\phi_h + \phi_S) + A_S \sin(\phi_h - \phi_S), \quad (1)
 \end{aligned}$$

4 *X. Qian*

where P_T is the target polarization, ϕ_h and ϕ_S are the azimuthal angles of the hadron momentum and the target spin relative to the lepton scattering plane (Fig. 1), Y is the normalized yield. A_C is the Collins moment, which probes the convolution of the chiral-odd transversity distribution h_1 and the chiral-odd Collins fragmentation function (FF)²⁷. A_S is the Sivers moment, which probes the convolution of the naive T-odd quark Sivers function f_{1T}^\perp ²⁸ and the unpolarized FF D_1 ^{29,22}. While the transversity function describes the correlation of the quark spin with the nucleon spin (the probability of finding a transversely polarized parton inside a transversely polarized nucleon), the Sivers function reveals the correlation of the quark OAM with the nucleon spin. In particular, authors of Ref. 30 provided constraints of quark angular momentum with world data of Sivers asymmetries and nucleon magnetic moments by assuming a connection between the generalized parton distribution E³¹ and the Sivers distribution. Since the Sivers function is odd under the naive time-reversal transformation, it was originally believed to vanish³². Recently, authors of Ref. 24 showed that a nonzero f_{1T}^\perp was possible due to QCD FSI between the struck quark and the residual nucleon system. It was further demonstrated that the Sivers function that appears in the Drell-Yan process is the same as the one in SIDIS, but with an opposite sign due to changes in the gauge link^{33,34}. The experimental tests of above relation are crucial in order to demonstrate the validity of the QCD factorization theorem.

Another example is the angular dependence of the beam-helicity double-spin asymmetry (DSA) A^{DSA} with a transversely polarized nucleon target and a longitudinal polarized lepton beam:

$$\begin{aligned} A_{LT}^{DSA}(\phi_h, \phi_S) &\equiv \frac{1}{P_B P_T} \frac{Y^+(\phi_h, \phi_S) - Y^-(\phi_h, \phi_S)}{Y^+(\phi_h, \phi_S) + Y^-(\phi_h, \phi_S)} \\ &\approx A_{LT}^{\cos(\phi_h - \phi_S)} \cos(\phi_h - \phi_S), \end{aligned} \quad (2)$$

where P_B is the polarization of the lepton beam, and $Y^\pm(\phi_h, \phi_S)$ are the normalized yields for beam helicity states of ± 1 . The first and second subscripts to A denote the respective polarization of beam and target (L, T, and U represent longitudinal, transverse, and unpolarized, respectively). Similar to the Collins and Sivers moments, the $A_{LT}^{\cos(\phi_h - \phi_S)}$ moment measures the convolution of g_{1T} and the unpolarized FF D_1 . g_{1T} has been calculated by lattice QCD^{35,36} and in various quark models^{37,38,39,40,41,42,43,44}. In general, g_{1T}^u (g_{1T}^d) is suggested to be positive (negative). In addition, g_{1T} is shown to be closely connected with other TMDs through models. First, the \mathbf{p}_T^2 -moment of g_{1T} is linked to the collinear g_1 PDF through a Wandzura-Wilczek-type approximation^{20,29} in the leading twist. Second, g_{1T}^q can be expressed as the combination of the quark transversity distribution h_1^q and the pretzelocity distribution $h_{1T}^{\perp q}$ within the QCD parton model⁴⁵. Last, g_{1T}^q is shown to be the same as $h_{1L}^{\perp q}$, but with an opposite sign in many models⁴⁶ as a consequence of a geometric relation and some initial lattice calculations^{35,36}.

On the experimental side, the HERMES and the COMPASS collaborations have performed pioneer work in measuring the SSA and the DSA. In particular, the

HERMES collaboration carried out the first SSA measurement in SIDIS on a transversely polarized proton target using e^\pm beams⁴⁷ at $Q^2 = 1.3 - 6.2 \text{ GeV}^2$. The COMPASS collaboration performed the SIDIS measurements with a muon beam on transversely polarized deuteron⁴⁸ and proton⁴⁹ targets at $Q^2 = 1.3 - 20.2 \text{ GeV}^2$. Both the HERMES⁵⁰ and the COMPASS⁴⁹ proton data show significantly positive π^+ Sivers moments and close to zero π^- Sivers moments, while results from the COMPASS deuteron data are consistent with zero. These measurements indicate a strong flavor dependence of the Sivers function⁵¹. In addition, though the HERMES and the COMPASS π^+ Sivers moments from their proton data are consistent in sign, potential discrepancies exist in magnitudes. These discrepancies might be attributed to the energy evolution of the Sivers function^{52,51}. For the Collins moment, large asymmetries were observed for both π^+ and π^- from the proton data, but with opposite sign. These results show that the “unfavored” Collins FF could be as large as the “favored” one³², which is also consistent with the measured asymmetries of the inclusive hadron pair production in the e^+e^- annihilation from the BELLE collaboration⁵³ (a direct measurement of product of Collins FFs). Furthermore, deuteron Collins asymmetries for π^+ and π^- are consistent with zero, which suggests a cancellation between proton and neutron. For the A_{LT} DSA, the preliminary results of the COMPASS collaboration from deuteron⁵⁴ and proton⁵⁵ are consistent with zero within uncertainties. The preliminary results of proton from the HERMES collaboration⁵⁶ are also mostly consistent with zero within uncertainties, except that a hint of positive π^+ moment is observed in the valence region.

Due to the nature of the electromagnetic interaction and charges of the u ($2/3$) and the d ($-1/3$) quarks, the SIDIS measurement of a proton target would be dominated by the contribution from u quarks. To shed light on the flavor structure of TMDs, it is important to perform the SSA and the DSA SIDIS measurements on a neutron target, which is more sensitive to the d -quark contribution. Since there is no stable free neutron target, polarized ^3He is commonly used as an effective polarized neutron target⁵⁷. The ^3He nucleus is uniquely advantageous in extraction of information on the neutron spin compared to the deuteron ($p+n$), since the ground state of ^3He is dominated by the S state, where the two protons' spins cancel each other.

3. Experiment E06-010

The E06-010 experiment⁵⁸ was carried out in Jefferson Lab (JLab) Hall A⁵⁹ from 2008/11 to 2009/02. Measuring the SSA and the DSA in the pion electroproduction $n(e, e' \pi^\pm)X$ on a transversely polarized ^3He target is the main object of this experiment. The results of SSA and DSA have been reported in Ref. 60 and Ref. 61, respectively. The beam energy of the longitudinally polarized electron was 5.89 GeV, the highest available at that time. The average beam current throughout the entire experiment was $12 \mu\text{A}$ corresponding to a polarized luminosity of $\sim 10^{36} \text{ N cm}^{-2} \text{ s}^{-1}$. Polarized electrons in the beam were excited from a superlattice GaAs photocathode

by a circularly polarized laser at the injector of the CEBAF accelerator. The electron beam-helicity was flipped at 30 Hz by changing the laser polarization with a Pockels cell. The beam polarization was periodically measured by a Møller polarimeter, and the average value is determined to be $(76.8 \pm 3.5)\%$. For SSA measurements, unpolarized beam was achieved by summing the two beam helicity states, with the residual beam charge asymmetry smaller than 100 ppm per 1-hour run.

The 40 cm long ^3He cell was filled with ~ 8 atms of ^3He and ~ 0.13 atms of N_2 (reducing depolarization effects) at room temperature. The Spin Exchange Optical Pumping (SEOP) of a Rb-K mixture was used to polarize the ^3He nuclei. The target polarization direction was controlled by three pairs of mutually orthogonal Helmholtz coils. Two orientations, vertical and horizontal polarizations in the plane transverse to the beam direction was chosen to maximize the ϕ_S coverage. The target spin was automatically flipped through the Adiabatic Fast Passage (AFP) every 20 minutes, while the target polarization was measured by the Nuclear Magnetic Resonance (NMR) in each flip. The known water NMR signal was used to calibrate the NMR measurements, and results were cross-checked with the Electron Paramagnetic Resonance (SPR) method. The average polarization was $(55.4 \pm 2.8)\%$.

Scattered electrons with momenta from 0.6-2.5 GeV were detected in the BigBite spectrometer at a central angle of 30° on the beam right. The BigBite spectrometer consisted of a large-opening dipole magnet in front of a detector stack including three sets of multi-wire drift chambers for tracking charged particles, a lead-glass calorimeter divided into preshower/shower sections for identifying electrons, and a scintillator plane between the preshower and shower for determining timing. The average solid angle was ~ 64 msr. The large out-of-plane angle acceptance of the BigBite (± 240 mrad) spectrometer was essential in maximizing the ϕ_h coverage of the experiment. The optics property of the BigBite magnet was calibrated using a multi-foil carbon target, a sieve slit collimator and the $^1\text{H}(e, e')p$ elastic scattering at incident energies of 1.2 and 2.4 GeV. The achieved angular and momentum resolutions were better than 10 mrad and 1%, respectively. A clean e^- identification was achieved using cuts on the preshower energy E_{ps} and the ratio E/p of the total shower energy to the momentum from optics reconstruction.

Coincident charged hadrons were detected in the High Resolution Spectrometer (HRS) at a central angle of 16° on the left side of beam and a central momentum of 2.35 GeV. The HRS detector package was configured to detect hadrons⁵⁹. The pion identification was achieved by combining a light gas Čerenkov, a lead glass calorimeter, an aerogel Čerenkov detector, and the time-of-flight (TOF) information.

SIDIS events were selected using cuts on the four-momentum transfer squared $Q^2 > 1 \text{ GeV}^2$, the hadronic final-state invariant mass $W > 2.3 \text{ GeV}$, and the mass of undetected final-state particles $W' > 1.6 \text{ GeV}$, assuming that the electron is scattered on a nucleon. The raw Collins and Sivers moments were obtained by fitting the asymmetries in 2-D (ϕ_h, ϕ_S) bins according to Eqn.(1). The raw A_{LT} moment was obtained by an unbinned maximum-likelihood method according to Eqn. (2).

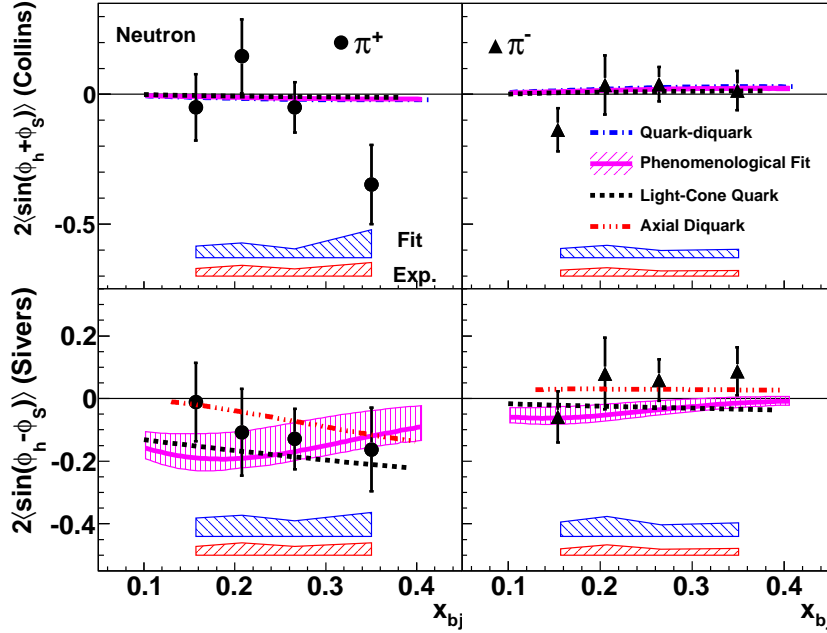


Fig. 2. (Color online) The extracted neutron Collins and Sivers moments with uncertainty bands for both π^+ and π^- electro-production from Ref. 60. See text for details.

Results were further cross-checked with both methods. The neutron SSA and DSA were extracted from the measured ^3He moments after correcting the directly measured N_2 dilution through

$$A_{^3\text{He}}^{SSA(DSA)} = P_n \cdot (1 - f_p) \cdot A_n^{SSA(DSA)} + P_p f_p \cdot A_p^{SSA(DSA)}. \quad (3)$$

Here, $P_n = 0.86^{+0.036}_{-0.02}$ ($P_p = -0.028^{+0.009}_{-0.004}$) is the neutron (proton) effective polarization⁶². The $f_p = \frac{2\sigma_p}{\sigma_{^3\text{He}}}$ is referred to as the proton dilution which is directly measured by comparing the yields of unpolarized hydrogen and ^3He targets. This approach was validated by a theoretical calculation⁶³.

The background in the SIDIS electron sample that comes from e^+/e^- pair production is the largest systematic uncertainty. This background was directly measured by reversing the polarity of the BigBite magnet to detect e^+ in identical conditions as e^- . Other experimental uncertainties include the K^\pm contamination in the π^\pm sample, effects of bin-centering/resolution/radiative corrections, the effect of the target collimator, the fluctuation of the target density, the false asymmetry due to the radiation damage to the BigBite preshower calorimeter, the contamination from the diffractive ρ meson production, the contamination from radiative tails of the exclusive electroproduction, and the effect of the π^\pm final state interaction. The quadrature sum of all above contributions is below 25% of the statistical

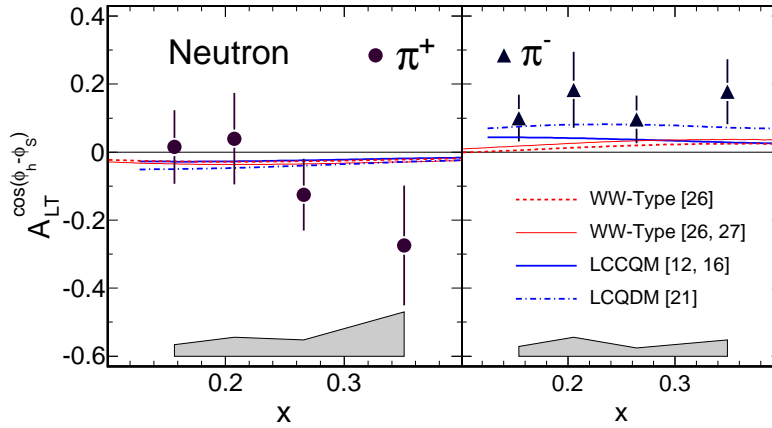


Fig. 3. (Color online) The neutron $A_{LT}^{\cos(\phi_h - \phi_S)}$ azimuthal asymmetry for positive (left) and negative (right) charged pions vs x from Ref. 61.

uncertainty.

The extracted neutron Collins and Sivers moments⁶⁰ are shown in the Fig. 2. The fitting systematic uncertainty (red band) is due to the neglect of other ϕ_h - and ϕ_S -dependent terms, such as the $2\langle\sin(3\phi_h - \phi_S)\rangle$, higher-twist terms including the $2\langle\sin\phi_S\rangle$ and the $2\langle\sin(2\phi_h - \phi_S)\rangle$, azimuthal modulations of the unpolarized cross section including the Cahn ($2\langle\cos\phi_h\rangle$) and the Boer-Mulders ($2\langle\cos(2\phi_h)\rangle$) terms. Collins moments are compared with the phenomenological fit⁶⁴, a light-cone quark model calculation^{65,66} and quark-diquark model^{67,68} calculations. With the Soffer's bound¹⁵, the phenomenological fit and model calculations predict rather small asymmetries which mostly agree with data, except the π^+ Collins moment at $x = 0.34$. Negative π^+ Sivers moments are favored by these data, while the π^- moments are close to zero. Within the parton model picture, such behavior is consistent with a negative d quark Sivers function, which has been suggested by predictions of the phenomenological fit⁶⁹ to the HERMES and the COMPASS data, a light-cone quark model calculation^{70,71}, and an axial diquark model calculation⁷².

The extracted neutron A_{LT} moments are shown in the Fig. 3. Beside aforementioned experimental systematic uncertainties, additional uncertainties include: the contamination from the DSA A_{LL} due to a 5%-20% longitudinal component of the target polarization with respect to the virtual-photon direction and the contribution from the A_{LT}^p estimated from the COMPASS preliminary data⁵⁵. Several model calculations, including WW-type approximations with parametrizations from Ref. 73 and Ref. 74, a light-cone constituent quark model (LCCQM)^{38,75}, and a light-cone quark-diquark model (LCDQM) evaluated using the second approach in the Ref. 43, are plotted as well. While the extracted $A_{LT}^n(\pi^+)$ is consistent with

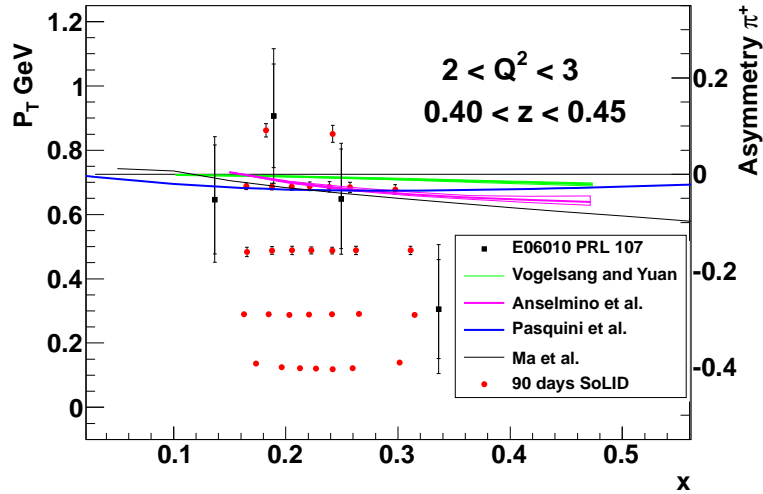


Fig. 4. (Color online) 12 GeV projections with the SoLID spectrometer and the polarized ^3He target of π^+ Collins asymmetries at $0.4 < z < 0.45$ and $2 \text{ GeV}^2 < Q^2 < 3 \text{ GeV}^2$. The Position of each projected point on the left y-axis represents the average P_T value of the corresponding kinematic bin. The statistical uncertainty of each point and magnitudes of theoretical calculations follow the right y-axis.

zero within uncertainties, the results of $A_{LT}^n(\pi^-)$ are consistent in sign with these model predictions but favor a larger magnitude. The sign of $A_{LT}^n(\pi^-)$ is opposite to the sign of the $A_{UL}^{\sin 2\phi_h}$ asymmetry in the π^+ production on the proton measured by the CLAS collaboration⁷⁶, which is predicted by many models⁴⁶.

4. Future Opportunities

The current generation of experiments including the HERMES, the COMPASS, and the E06-010 play important roles in exploring TMDs. However, compared to the collinear unpolarized and longitudinal polarized functions (f_1 and g_1) which depend on x and Q^2 only, TMDs are much less understood due to their multi-dimensional nature (x , Q^2 and the quark transverse momentum p_T). For example, the kinematics of x , z and P_T are always strongly correlated in all existing experiments, and results are usually shown in one dimensional format (x , z or P_T) with integration over the other two variables. Furthermore, many assumptions, such as a Gaussian approximation of p_T dependence, have been adopted in the global fit to limit the total number of parameters. Therefore, in order to improve our understanding on TMDs and to reduce aforementioned theoretical assumptions, it is important to perform precision measurements in multiple dimensions.

Jefferson Lab is upgrading its incident electron beam energy to 12 GeV, which provides unique opportunities to carry out measurements of semi-inclusive hadron yields from deep-inelastic scattering. Two experiments^{77,78} have been ap-

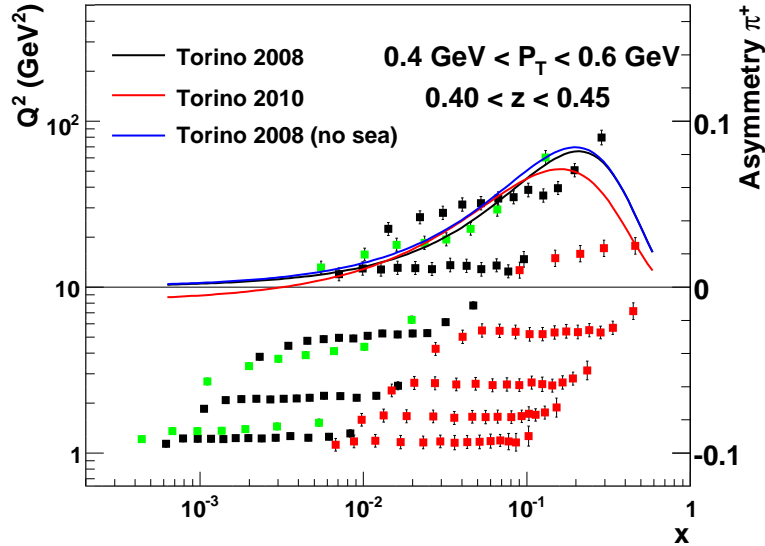


Fig. 5. (Color online) Projections of the Siverts asymmetry of the π^+ electro-production off the proton⁸⁴ in a P_T and z bin out of 40 bins along with various calculated asymmetries. The black, green, and red dots represent the 11+60 GeV, the 11+100 GeV, and the 3+20 GeV EIC configurations, respectively. The integrated luminosity is assumed to be $3.1 \times 10^{40} \text{ cm}^{-2}$, $9.3 \times 10^{40} \text{ cm}^{-2}$, and $3.1 \times 10^{40} \text{ cm}^{-2}$ for 3+20 GeV, 11+60 GeV and 11+100 GeV configurations, respectively. The x -axis represents Bjorken x , and the left y -axis represents Q^2 . The position of each point represents the position of the kinematic bin in the x - Q^2 phase space. The error bar of each point and magnitudes of calculated asymmetries follow the right y -axis.

proved with the same polarized ^3He target and a large acceptance solenoid device (SoLID)⁷⁹. The fixed-target kinematics allows for a probe of the interesting high x region (0.05-0.65), which is essential in determining quark tensor charges. In addition, the full azimuthal angular coverage of SoLID results in a significant reduction of systematic uncertainties of the luminosity, detection efficiencies, etc., which is essential for high precision measurements. The projected results for π^+ Collins asymmetry are shown in the Fig. 4 for one typical kinematic bin (48 bins in total), $0.4 < z < 0.45$, $2 \text{ GeV}^2 < Q^2 < 3 \text{ GeV}^2$. Theoretical predictions of the Collins asymmetries from Anselmino *et al.*⁸⁰, Vogelsang and Yuan⁸¹, Ma *et al.*⁸², and Psalini *et al.*³⁸ are shown as well. The results of E06-010⁶⁰ are shown as black points. In addition, an experiment with a transversely polarized proton target⁸³ is proposed to achieve the flavor separation. These next generation experiments will provide a high precision measurement of various SSA and DSA asymmetries in the valence quark region.

Compared to the fixed target experiments, an electro-ion collider (EIC) will be able to probe much larger phase space in x , Q^2 and P_T due to a much large center of mass energy. In particular, an EIC is an ideal machine to study TMDs for

sea quarks and gluons at low x . The large Q^2 coverage will allow a study of the evolution of TMDs as well as various higher twist effects. In addition, the large hadron transverse momentum P_T coverage will allow a study of SSA and DSA phenomenon at high P_T , where NLO QCD processes dominate. Furthermore, an EIC enables the capability to detect open charm mesons. These new probes open a window to study gluon distribution functions⁸⁴. For example, SSAs of the open-flavor (anti)D meson production in the DIS regime provide a unique opportunity to measure tri-gluon correlation functions^{85,86}, which are closely connected to the gluon's transverse motion and the color coherence inside a transversely polarized nucleon. Summaries of the physics potential of an EIC are presented in the Ref. 84 and the Ref. 87. Fig. 5 shows the expected projection of the π^+ Sivers asymmetry with a proton beam at a high luminosity EIC in the kinematics bin of $0.4 < z < 0.45$ and $0.4 \text{ GeV} < P_T < 0.6 \text{ GeV}$. Together with the projection, a few calculations of the Sivers asymmetry from Ref. 80 and Ref. 88 are presented. Fig. 6 shows the projection for the D transverse SSA measurement for a running time of 144 days with a proton beam at a luminosity of $3 \times 10^{34} \text{ cm}^{-2} \text{ s}^{-1}$ together with a theoretical prediction from the Ref. 85. With the 12 GeV upgrade and a high luminosity electron-ion collider, the knowledge of TMDs of gluons and quarks can be greatly advanced, and would ultimately improve our understanding of TMDs from the first principle of QCD.

5. Summary

The Jefferson Lab E06-010 experiment measured the neutron SSA and DSA for the first time through pion electroproduction in the DIS region with a transversely polarized ^3He target. These data provide valuable information about nucleon TMDs, which describes not only nucleon structure in 3-D momentum space, but also provide insights to the dynamics of QCD in the confinement region. The precision measurements at 12-GeV Jefferson Lab and a future EIC would ultimately realize the multi-dimensional mapping of TMDs, which will bring our current understanding of the nucleon structure to a completely new level.

Acknowledgments

This work was supported in part by Caltech, U.S. Department of Energy (DOE) under contract number DE-FG02-03ER41231, the National Science Foundation, and by DOE contract number DE-AC05-06OR23177, under which the Jefferson Science Associates (JSA) operates the Thomas Jefferson National Accelerator Facility.

References

1. D. J. Gross and F. Wilczek, Phys. Rev. Lett. **30**, 1343 (1973).
2. H. D. Politzer, Phys. Rev. Lett. **30**, 1346 (1973).
3. F. Caola, S. Forte, and J. Rojo, Nucl. Phys. **A854**, 32 (2011).

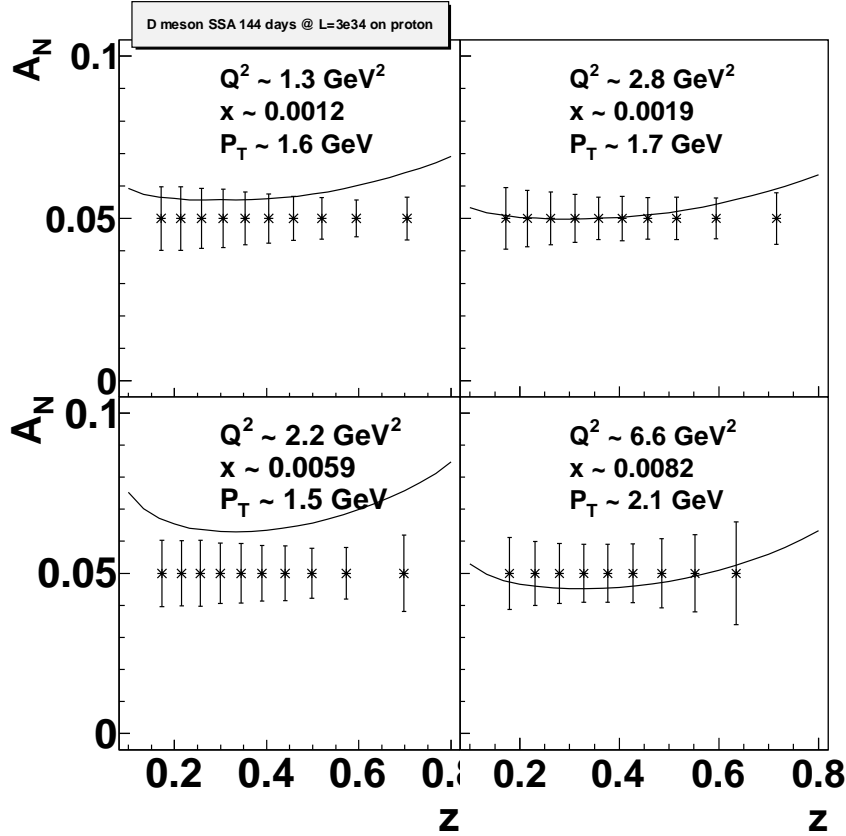


Fig. 6. The projected results⁸⁷ on the transverse SSA of the D meson production. The data are binned 2-by-2 in terms of x and Q^2 . Within each x - Q^2 bin, projections are plotted with z . The central kinematics are listed in each panel.

4. S. E. Kuhn, J.-P. Chen, and E. Leader, Prog. Part. Nucl. Phys. **63**, 1 (2009).
5. K. Hidaka, E. Monsay and D. Sivers, Phys. Rev. **D19**, 1503 (1979).
6. J. P. Ralston and D. E. Soper, Nucl. Phys. **B152**, 109 (1979).
7. R. L. Jaffe and X. Ji, Phys. Rev. Lett. **67**, 552 (1991).
8. M. Gockeler *et al.*, Phys. Lett. **B627**, 113 (2005).
9. H.-X. He and X. Ji, Phys. Rev. **D52**, 2960 (1995).
10. V. Barone *et al.*, Phys. Lett. **B390**, 287 (1997).
11. B.-Q. Ma and I. Schmidt, J. Phys. **G24**, 71, (1998).
12. B. Pasquini *et al.*, Phys. Rev. **D72**, 094029 (2005).
13. M. Wakamatsu, Phys. Lett. **B653**, 398 (2007).
14. I. C. Cloet *et al.*, Phys. Lett. **B659**, 214 (2008).
15. J. Soffer, Phys. Rev. Lett. **74**, 1292 (1995).
16. S. Kumano and M. Miyama, Phys. Rev. **D56**, 2504 (1997).
17. A. Hayashigaki *et al.*, Phys. Rev. **D56**, 7350 (1997).
18. W. Vogelsang, Phys. Rev. **D57**, 1886 (1998).

19. J. P. Ralston, arXiv:0810.0871 (2008).
20. P. J. Mulders and R. D. Tangerman, Nucl. Phys. **B461**, 197 (1996).
21. D. Boer, P. J. Mulders, Phys. Rev. **D57**, 5780 (1998).
22. A. Bacchetta *et al.*, JHEP **02**, 093 (2007).
23. P. V. Pobylitsa, hep-ph/0301236.
24. S. J. Brodsky, D. S. Hwang and I. Schmidt, Phys. Lett. **B530**, 99 (2002).
25. X. Ji, J.-P. Ma, and F. Yuan, Nucl. Phys. **B652**, 383 (2003).
26. A. Bacchetta *et al.*, Phys. Rev. **D70**, 117504 (2004).
27. J. C. Collins, Nucl. Phys. **B396**, 161 (1993).
28. D. Sivers, Phys. Rev. **D41**, 83 (1990).
29. A. M. Kotzinian and P. J. Mulders, Phys. Rev. **D54**, 1229 (1996).
30. A. Bacchetta and M. Radici, arXiv:1107.5755.
31. X. Ji, Phys. Rev. Lett. **78**, 610 (1997).
32. J. C. Collins, Nucl. Phys. **B396**, 161 (1993).
33. J. C. Collins, Phys. Lett. **B536**, 43 (2002).
34. S. J. Brodsky *et al.*, Nucl. Phys. **B642**, 344 (2002).
35. P. Hagler *et al.*, Europhys. Lett. **88**, 61001 (2009).
36. B. U. Musch *et al.*, Phys. Rev. **D83**, 094507 (2011).
37. R. Jakob, P. Mulders, and J. Rodrigues, Nucl. Phys. **A626**, 937 (1997).
38. B. Pasquini, S. Cazzaniga, and S. Boffi, Phys. Rev. **D78**, 034025 (2008).
39. A. Kotzinian, arXiv:0806.3804 (2008).
40. A. V. Efremov *et al.*, Phys. Rev. **D80**, 014021 (2009).
41. H. Avakian *et al.*, Phys. Rev. **D81**, 074035 (2010).
42. A. Bacchetta *et al.*, Euro. Phys. J. **A45**, 373 (2010).
43. J. Zhu and B.-Q. Ma, Phys. Lett. **B696**, 246 (2011).
44. A. V. Efremov *et al.*, J. Phys. Conf. Ser. **295**, 012052 (2011).
45. E. Di Salvo, Mod. Phys. Lett. **A22**, 1787 (2007).
46. C. Lorce and B. Pasquini, Phys. Rev. **D84**, 034039 (2011).
47. A. Airapetian *et al.*, Phys. Rev. Lett. **94**, 012002 (2005).
48. M. Alekseev *et al.*, Phys. Lett. **B673**, 127 (2009).
49. M. Alekseev *et al.*, Phys. Lett. **B692**, 240 (2010).
50. A. Airapetian *et al.*, Phys. Rev. Lett. **103**, 152002 (2009).
51. M. Anselmino, M. Boglione, and S. Melis, arXiv:1204.1239 (2012).
52. S. M. Aybat *et al.*, Phys. Rev. **D85**, 034043 (2012).
53. R. Seidl *et al.* Phys. Rev. Lett. **96**, 232002 (2006).
54. B. Parsamyan (COMPASS), Euro. Phys. J. Special Topics **162**, 89 (2008).
55. B. Parsamyan (COMPASS), J. Phys. Conf. Ser. **295**, 012046 (2011).
56. L. L. Pappalardo and M. Diefenthaler (HERMESS), arXiv:1107.4227 (2011).
57. F. Bissey *et al.* Phys. Rev. **C65**, 064317 (2002).
58. Jefferson Lab E06010, Spokesperson: J.-P. Chen, E. Cisbani, H. Gao, X. Jiang, and J.-C. Peng.
59. J. Alcorn *et al.*, Nucl. Instr. and Meth. **A522**, 294 (2004).
60. X. Qian *et al.* Phys. Rev. Lett. **107**, 072003 (2011).
61. J. Huang *et al.* Phys. Rev. Lett. **108**, 052001 (2012).
62. X. Zheng *et al.*, Phys. Rev. **C70**, 065207 (2004).
63. S. Scopetta, Phys. Rev. **D75**, 054005 (2007).
64. M. Anselmino *et al.*, Phys. Rev. **D75**, 054032 (2007).
65. S. Boffi *et al.*, Phys. Rev. **D79**, 094012 (2009).
66. B. Pasquini, S. Cazzaniga and S. Boffi, Phys. Rev. **D78**, 034025 (2008).
67. J. She and B. Q. Ma, Phys. Rev. **D83**, 037502 (2011).

14 X. Qian

68. B. Q. Ma, I. Schmidt, J. J. Yang, Phys. Rev. **D65**, 034010 (2002).
69. M. Anselmino *et al.*, Phys. Rev. **D72**, 094007 (2005).
70. S. Arnold *et al.*, arXiv:0805.2137 (2008).
71. B. Pasquini and P. Schweitzer, Phys. Rev. **D83**, 114044 (2011).
72. L. P. Gamerg *et al.* Phys. Rev. **D77**, 094016 (2008).
73. A. Kotzinian, B. Parsamyan, and A. Prokudin, Phys. Rev. **D73**, 114017 (2006)
74. A. Prokudin *private communications*.
75. S. Boffi *et al.*, Phys. Rev. **D79**, 094012 (2009).
76. H. Avakian *et al.* (CLAS), Phys. Rev. Lett. **105**, 262002 (2010).
77. Jefferson Lab E12-10-006, Spokesperson: J.-P. Chen, H. Gao, X. Jiang, X. Qian, J.-C. Peng.
78. Jefferson Lab E12-11-007, Spokesperson: J.-P. Chen, J. Huang, Y. Qiang, W. B. Yan.
79. H. Gao *et al.* Enr. Phys. J. Plus **126**, 2 (2011).
80. M. Anselmino and A. Prokudin, *private communications*.
81. W. Vogelsang and F. Yuan, *private communications*.
82. Y. Huang, J. She and B.-Q. Ma, Phys. Rev. **D76**, 034004 (2007).
83. Jefferson Lab PR12-11-108, Spokesperson: K. Allada, J.-P. Chen, X. M. Li, H. Gao, Z.-E. Meziani.
84. M. Anselmino *et al.* Euro. Phys. J. **A47**, 35 (2011).
85. Z. B. Kang and J. W. Qiu, Phys. Rev. **D78**, 034005 (2008).
86. H. Beppu *et al.*, Phys. Rev. **D82**, 054005 (2010).
87. D. Boer *et al.* arXiv:1108.1713 (2011).
88. M. Anselmino *et al.*, Euro. Phys. J. **A39**, 89 (2009).